Performance limit of daytime radiative cooling in warm humid environment

Cite as: AIP Advances **8**, 055124 (2018); https://doi.org/10.1063/1.5030156
Submitted: 20 March 2018 • Accepted: 15 May 2018 • Published Online: 23 May 2018

Takahiro Suichi, Atsushi Ishikawa, Yasuhiko Hayashi, et al.

Performance limit of daytime radiative cooling in warm humid environment

Takahiro Suichi, Atsushi Ishikawa,[a] Yasuhiko Hayashi, and Kenji Tsuruta
Department of Electrical and Electronic Engineering, Okayama University, Okayama, Okayama 700-8530, Japan

(Received 20 March 2018; accepted 15 May 2018; published online 23 May 2018)

Daytime radiative cooling potentially offers efficient passive cooling, but the performance is naturally limited by the environment, such as the ambient temperature and humidity. Here, we investigate the performance limit of daytime radiative cooling under warm and humid conditions in Okayama, Japan. A cooling device, consisting of alternating layers of SiO_2 and poly(methyl methacrylate) on an Al mirror, is fabricated and characterized to demonstrate a high reflectance for sunlight and a selective thermal radiation in the mid-infrared region. In the temperature measurement under the sunlight irradiation, the device shows 3.4 °C cooler than a bare Al mirror, but 2.8 °C warmer than the ambient of 35 °C. The corresponding numerical analyses reveal that the atmospheric window in $\lambda = 16 \sim 25$ μm is closed due to a high humidity, thereby limiting the net emission power of the device. Our study on the humidity influence on the cooling performance provides a general guide line of how one can achieve practical passive cooling in a warm humid environment.
https://doi.org/10.1063/1.5030156

Radiative cooling, which is the most fundamental Earth's cooling mechanism, is a promising phenomenon for improving energy efficiency of cooling and outdoor devices, such as air conditioners and photovoltaic cells.[1–7] The heat from terrestrial objects is eventually radiated out to cold outer space by the thermal radiation through the infrared (IR) atmospheric window. Passive radiative cooling below the ambient temperature is practically possible with a selective thermal emitter, which has a strong IR absorption within the atmospheric window.[1–3,8,9] Such a cooling mechanism, however, is naturally difficult to realize during the daytime, since the absorbed power from the incident sunlight is much larger than the thermal radiation power at room temperature. On the other hand, nanophotonic structures, e.g., metallodielectric multilayers, can overcome this fundamental limitation by tailoring their spectral responses and the resultant photonic-thermal properties. Recent development of nanophotonic cooling devices has shown to achieve daytime radiative cooling below the ambient temperature by near-perfectly reflecting the sunlight, while selectively emitting the mid-infrared (MIR) radiation.[10,11] For scalable and practical daytime radiative cooling, simple yet powerful structures have been also proposed, such as SiO_2 microspheres dispersed in a polymer matrix and a polymer-coated SiO_2 wafer.[12,13]

Although several new designs of the cooling device have been demonstrated so far, these approaches have mainly focused on improving the thermal radiation efficiency and device scalability, but few examples precisely assess the humidity influence on the cooling performance. Precipitable water vapor (PWV) is an important parameter of humidity to represent the depth of water that would result if all the vapor in a column of the atmosphere above a certain location were condensed as rain. Recent successful demonstrations of daytime radiative cooling have been performed mostly in dry regions of North America where their PWV is about $1 \sim 10$ mm. In such a dry environment,

[a]Electronic mail: a-ishikawa@ec.okayama-u.ac.jp.

the atmospheric window opens not only in $\lambda = 8 \sim 13$ μm, but also in $\lambda = 16 \sim 25$ μm, making the efficient thermal radiation possible.[10,12] On the other hand, warm regions, such as Asian countries including Japan, usually experience a high PWV more than 20 mm.[14] In such a warm humid environment, the cooling performance naturally becomes lower and is even limited due to the IR absorption of water vapor; therefore not only the improvement of the thermal radiation, but also the humidity influence has to be carefully considered.

Here, we investigate the performance limit of daytime radiative cooling under warm and humid conditions in Okayama, Japan. Specifically, we study the photonic-thermal properties of a metallodielectric multilayer structure to exhibit a high reflectance for sunlight and a selective thermal radiation in the MIR region. In the temperature measurement as well as the numerical analyses, we demonstrate deterioration of the cooling performance by a high humidity, which is significant in Asian countries. Our study on the humidity influence on the daytime radiative cooling provides essential insight for developing practical cooling devices in a warm humid environment.

Figure 1(a) shows a schematic cross-section of a metallodielectric multilayer structure of the cooling device. It consists of alternating layers of SiO_2 and poly(methyl methacrylate) (PMMA) on an Al mirror. The layer number and thickness were determined based on simulated annealing method combined with a photonic-thermal analysis such that the cooling performance became as high as possible.[15,16] The Al mirror provides a high reflectance for the sunlight extending from the ultraviolet (UV) to near-infrared (NIR) region. The SiO_2 layer, on the other hand, exhibit a selective thermal radiation in the MIR region based on a strong phonon resonance of the SiO_2. The top SiO_2 and PMMA layers were optimally designed to exhibit a multiple interference effect for an enhanced thermal radiation.

Figure 1(b) shows a photograph of the fabricated multilayer structure on a SiO_2 substrate with a total area of 25×25 mm^2. The fabrication process started with a resistive heating evaporation of a 70-nm Al film onto the SiO_2 substrate. Using a reactive evaporation where SiO steam is transformed into SiO_2 in oxygen gas, a 1444-nm SiO_2 layer was deposited on the Al film surface. The sample was then completed by spin-coating of a 500-nm PMMA layer, followed by a 172-nm SiO_2 layer deposition. The thickness of each layer was determined by using an optical surface profiler (Zygo, New View 7300) with a height resolution of less than 0.1 nm. A bare Al mirror was also prepared for the reference in the same manner.

To evaluate the optical response of the fabricated device, the normal reflectance (R) was firstly measured in the solar ($\lambda = 0.28 \sim 2.5$ μm) and IR ($\lambda = 2.5 \sim 25$ μm) regions by using an UV-Vis-NIR spectrometer (JASCO, V-670EX and SLM-736) and a Fourier-transform infrared spectrometer (JASCO, FT/IR-4200 and RF-81S), respectively. The spectral emissivity in Figure 2(a) was then obtained based on Kirchhoff's law ($\epsilon = A = 1 - R$). The corresponding simulation result was obtained by simply solving the Fresnel equations for the multilayer structure with the empirical optical constants for SiO_2, PMMA, and Al.[17–22] Note that the angle-dependency of the device's emissivity was considered only in the simulation, not in the experiment. However, the additional simulation result (not shown here) indicated that the difference of the device's emissivity was negligible between the cases with/without considering the angle-dependency in the experiment. In Fig. 2(a), the AM1.5G

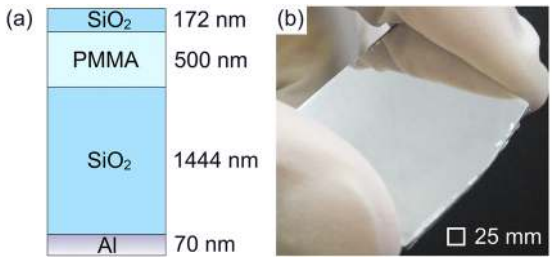

FIG. 1. (a) Schematic cross-section of a metallodielectric multilayer structure of the radiative cooling device. It consists of alternating layers of SiO_2 and PMMA on an Al mirror, which were optimally designed to exhibit a multiple interference effect for an enhanced thermal radiation. (b) Photograph of the fabricated multilayer structure on a SiO_2 substrate with a total area of 25×25 mm^2.

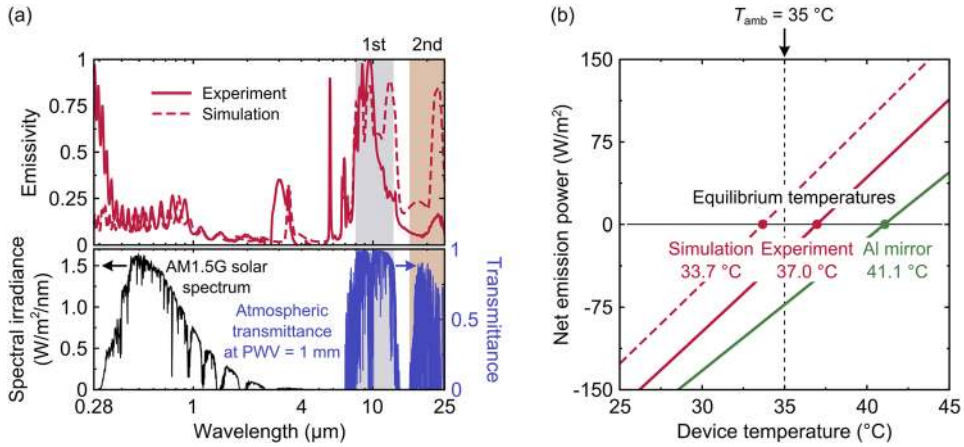

FIG. 2. (a) Experimentally measured (solid red) and numerically simulated (dashed red) spectral emissivity of the device. The AM1.5G solar spectrum (black) and atmospheric transmittance (blue) are also shown in (a) for the reference. The shaded regions represent the 1st (gray, λ = 8 ~ 13 μm) and 2nd (brown, λ = 16 ~ 25 μm) atmospheric windows. (b) Net emission power for the measured and simulated emissivity of the device at the ambient temperature of 35 °C. The same for a bare Al mirror (green) is also plotted for comparison. Each point at the intersection of the curves with the horizontal axis of P_{net} = 0 indicates the equilibrium temperatures of each case.

solar spectrum and atmospheric transmittance at PWV = 1 mm are also shown for the reference.[23–25] Note that the atmospheric transmittance consists of the 1st (λ = 8 ~ 13 μm) and 2nd (λ = 16 ~ 25 μm) windows with the averaged transmittance of 0.89 and 0.43, respectively.

In the experimental result (solid red), a low emissivity, i.e., a high reflectance, in the solar region and a selective emission peak in the MIR region were clearly observed. These observations are fairly supported by the simulation result (dashed red), exhibiting the averaged sunlight reflectance of 0.89 and the averaged emissivity in the 1st and 2nd windows of 0.72 and 0.44, except for minor discrepancies; i) the emission peaks in the 1st and 2nd windows became narrower and ii) the absorption in the UV region increased in the experimental result. These discrepancies can be explained by the composition change of the SiO_2 layer in the reactive evaporation where SiO steam was not fully transformed to SiO_2.[2]

To analyze the heat balance of the device, the equilibrium temperature was characterized by calculating the following net emission power:

$$P_{net} = P_{rad}(T_{dev}) - P_{sun} - P_{atm}(T_{amb}) - P_{cc}(T_{dev}, T_{amb}) \quad (1)$$

where $P_{rad}(T_{dev})$ is the radiated power from the device at the device temperature T_{dev}, P_{sun} is the absorbed power from the incident sunlight, $P_{atm}(T_{amb})$ is the absorbed power from the atmospheric thermal radiation at the ambient temperature T_{amb}, and $P_{cc}(T_{dev},T_{amb})$ is the absorbed power from the surroundings by heat conduction and convection.[10,11] Fig. 2(b) shows the calculated P_{net} for the measured and simulated emissivity in Fig. 2(a) at the ambient temperature of 35 °C. In Fig. 2(b), the result for a bare Al mirror was also shown for comparison. In the calculation, empirical values, a solar irradiance of 900 W/m^2 and a non-radiative heat transfer coefficient of 12 W/m^2/K were used to emulate the experimental condition.

As the device temperature increased, P_{net} linearly increased from a negative to positive value where the device absorbs (radiates) power from (to) the surroundings at a low (high) temperature. Each point at the intersection of the curves with the horizontal axis of P_{net} = 0 indicates the equilibrium temperatures of each case; 33.7 °C, 37.0 °C, and 41.1 °C for the simulation, experiment, and Al mirror, respectively. Compared to the ambient temperature of 35 °C, the simulation result (dashed red) was 1.3 °C cooler, but the experimental result (solid red) was 2.0 °C warmer than the ambient. This was due to the decrease of the MIR emissivity and the increase of the UV absorption, as shown in Fig. 2(a). Although the sub-ambient cooling cannot be expected for the fabricated device, it is still expected to exhibit 4.1 °C cooler than the Al mirror under the current condition. Since the Al

mirror has a high sunlight reflectance comparable to the device but a near-zero MIR emissivity, the temperature difference between the device and Al mirror represents a cooling capability of the device by the selective thermal radiation.

The cooling performance of the device was experimentally characterized by measuring its temperature under the sunlight irradiation on an occasionally-cloudy early-summer day. Figure 3(a) shows a photograph of an experimental setup on the roof of our building in Okayama, Japan (34°N, 134°E, at an altitude of 20 m). The fabricated device and reference Al mirror were placed in a wind shield to suppress their temperature fluctuation by wind. Fig. 3(b) shows a schematic cross-section of the wind shield, consisting of an optically-transparent acrylic sample chamber and an aluminized wood frame, to minimize the increase of the internal temperature due to the sunlight.[11] The top face of the shield was covered by a low-density polyethylene film to transmit both the sunlight and the MIR radiation. The wind shield was tilted by 12° toward the sun at noon to realize the normal incidence of the sunlight to the samples, which is the same condition as the simulation. The temperatures of the samples were simultaneously measured by using thermocouples, as shown in Fig. 3(c). Fig. 3(d) shows an IR thermal image of the samples captured by using an IR thermal imager (FLIR Systems, TG165) with a sensitivity at $\lambda = 8 \sim 14$ μm, demonstrating the device (yellow-green) exhibited a relatively high emissivity in the 1st atmospheric window compared to the Al mirror (blue).

Figure 4 shows the experimentally measured temperatures of the Al mirror, device, and ambient air during the noontime with a measurement time interval of 1 min. The measured solar irradiance was also shown in Fig. 4 where it occasionally dropped due to cloud, but it showed 867 W/m^2 on average. Following the fluctuation of the irradiance, the sample temperatures also fluctuated slowly with a time delay due to a finite heat capacity of the SiO_2 substrate. On the other hand, the ambient with a large heat capacity remained around 35 °C, which is the typical summer temperature in Japan.

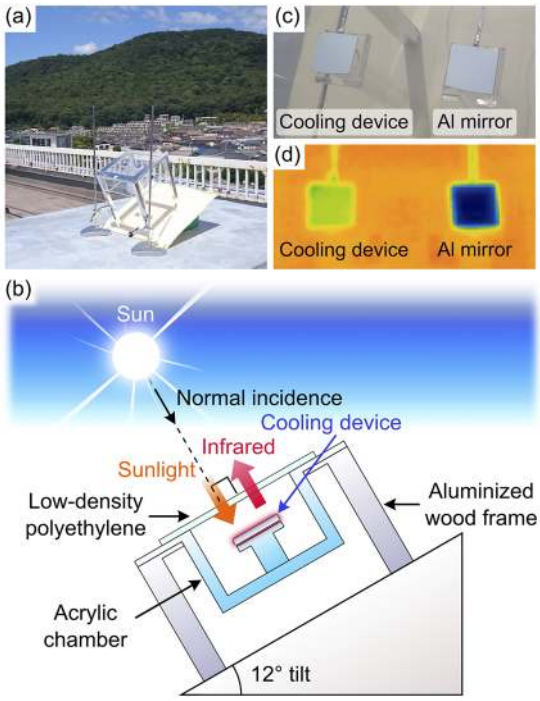

FIG. 3. (a) Photograph of an experimental setup on the roof of our building in Okayama, Japan. (b) Schematic cross-section of the wind shield, consisting of an optically-transparent acrylic sample chamber and aluminized wood frame, to minimize the increase of the internal temperature due to the sunlight. The top face of the shield was covered by a low-density polyethylene film to transmit both the sunlight and the MIR radiation. The wind shield was 12° titled toward the sun at noon to realize the normal incidence of the sunlight to the samples. (c) Close-up photograph and (d) IR thermal image of the samples in the wind shield where the temperature of each structure was simultaneously measured by thermocouples.

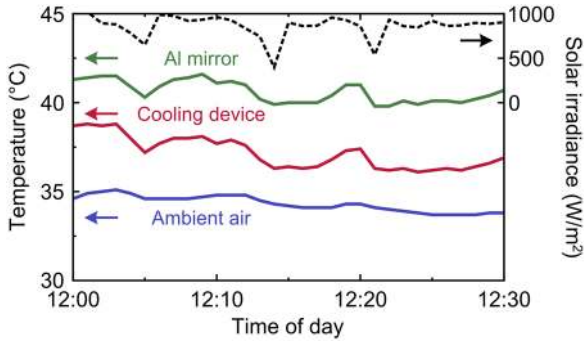

FIG. 4. Experimentally measured temperatures of the Al mirror (green), device (red), and ambient air (blue) during the noontime with a measurement time interval of 1 min. The measured solar irradiance (black) is also shown for the reference where it occasionally dropped due to cloud, but it showed 867 W/m^2 on average.

On average, the device was 2.8 °C warmer than the ambient, but 3.4 °C cooler than the Al mirror. Compared to the theoretical prediction at PWV = 1 mm in Fig. 2(b), the cooling capability of the device was further deteriorated due to a high humidity in the experiment.

To better understand the humidity influence on the cooling performance, the equilibrium temperature of the device was calculated as a function of the PWV using Eq. (1) with the simulated emissivity in Fig. 2(a). Figure 5 shows the calculated device temperature at the ambient temperature of 35 °C and the averaged atmospheric transmittance of the 1st and 2nd windows. In the upper horizontal axis of Fig. 5, the corresponding latitude is also shown.[14] At PWV = 1 mm, which is the driest case in the world, the atmosphere had a fairly good transmittance not only in the 1st window (T_1 = 0.89), but also in the 2nd window (T_2 = 0.43). Therefore, the device efficiently emitted the MIR radiation through both 1st and 2nd windows, and it exhibited 1.3 °C cooler than the ambient. As the PWV increased, on the other hand, the transmittance of the 2nd window drastically decreased, thereby limiting the net emission power of the device due to the enhancement of the atmospheric thermal radiation. At PWV = 20 mm, which is a typical value on early-summer days in Japan,[26] the transmittance of the 1st window remained high (T_1 = 0.79), but the 2nd window was almost closed (T_2 = 0.03) by the IR absorption of water vapor. As a result, the device at PWV = 20 mm exhibited 2.0 °C warmer than that at PWV = 1 mm, corresponding to 0.7 °C warmer than the ambient. Note that the typical temperature-dependency was also observed in the additional simulation result (not shown here) where the cooling performance of the device was improved (deteriorated) as the ambient temperature increased (decreased).[9]

Warm regions, such as Asian countries below the latitude of 30°, usually experience a high PWV more than 20 mm; therefore, the cooling performance of the device becomes much lower and is even

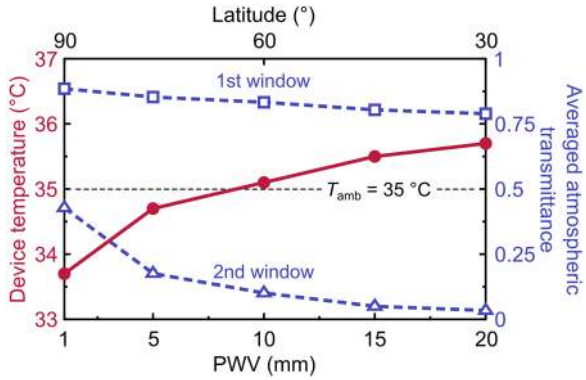

FIG. 5. Equilibrium temperature of the device (red) at the ambient temperature of 35 °C as a function of the PWV. The corresponding latitude is shown in the upper horizontal axis. The averaged atmospheric transmittance of the 1st (blue square) and 2nd (blue triangle) windows are also shown, revealing that the 2nd window was closed at a high PWV.

limited by the loss of the 2nd window. Especially, if the device has a high emissivity in the 2nd window, the device is heated up by the radiative heat exchange from the warm atmosphere ($T_{amb} > T_{dev}$).[9] In such a warm humid environment, the spectral emissivity of the device must be maximized only in the 1st window, but minimized elsewhere including the 2nd window to achieve practical daytime radiative cooling.

In conclusion, the performance limit of daytime radiative cooling was experimentally and numerically investigated under warm and humid conditions in Okayama, Japan. The cooling device, consisting of alternating layers of SiO_2 and PMMA on an Al mirror, was fabricated and characterized to exhibit a high reflectance for the sunlight and a selective thermal radiation in the MIR region. In the temperature measurement as well as the numerical analyses, we demonstrated that the 2nd atmospheric window was almost closed at PWV = 20 mm by the IR absorption of water vapor, giving a more than 2.0 °C increase of the device temperature compared to the case at PWV = 1 mm. Hence, the cooling device in such a warm humid environment must be designed to exhibit maximized emissivity only in the 1st window, but minimized one elsewhere including the 2nd window to achieve practical daytime radiative cooling.

This work was supported in part by the JSPS KAKENHI Grant Number 15KK0237. The nanofabrication in this work was performed at the Division of Instrumental Analysis, Okayama University.

[1] C. G. Granqvist and A. Hjortsberg, Appl. Phys. Lett. **36**, 139 (1980).
[2] C. G. Granqvist and A. Hjortsberg, J. Appl. Phys. **52**, 4205 (1981).
[3] C. G. Granqvist, Appl. Opt. **20**, 2606 (1981).
[4] E. A. Goldstein, A. P. Raman, and S. Fan, Nat. Energy **2**, 17143 (2017).
[5] L. Zhu, A. Raman, K. X. Wang, M. A. Anoma, and S. Fan, Optica **1**, 32 (2014).
[6] L. Zhu, A. P. Raman, and S. Fan, Proc. Natl. Acad. Sci. U.S.A. **112**, 12282 (2015).
[7] W. Li, Y. Shi, K. Chen, L. Zhu, and S. Fan, ACS Photon. **4**, 774 (2017).
[8] M. M. Hossain, B. Jia, and M. Gu, Adv. Opt. Mater. **3**, 1047 (2015).
[9] Z. Chen, L. Zhu, A. Raman, and S. Fan, Nat. Commun. **7**, 13729 (2016).
[10] E. Rephaeli, A. Raman, and S. Fan, Nano Lett. **13**, 1457 (2013).
[11] A. P. Raman, M. A. Anoma, L. Zhu, E. Rephaeli, and S. Fan, Nature **515**, 540 (2014).
[12] Y. Zhai, Y. Ma, S. N. David, D. Zhao, R. Lou, G. Tan, R. Yang, and X. Yin, Science **355**, 1062 (2017).
[13] J.-I. Kou, Z. Jurado, Z. Chen, S. Fan, and A. J. Minnich, ACS Photon **4**, 626 (2017).
[14] G. G. Amenu and P. Kumar, Bull. Amer. Meteor. Soc. **86**, 245 (2005).
[15] S. Kirkpatrick, C. D. Gelatt, Jr., and M. P. Vecchi, Science **220**, 671 (1983).
[16] V. Černý, J. Optim. Theory Appl. **45**, 41 (1985).
[17] D. De Sousa Meneses, M. Malki, and P. Echegut, J. Non-Cryst. Solids **352**, 769 (2006).
[18] R. Kitamura, L. Pilon, and M. Jonasz, Appl. Opt. **46**, 8118 (2007).
[19] V. M. Zolotarev, B. Z. Volchek, and E. N. Vlasova, Opt. Spectrosc. **101**, 716 (2006).
[20] N. Sultanova, S. Kasarova, and I. Nikolov, Acta Phys. Pol. A **116**, 585 (2009).
[21] A. D. Rakić, A. B. Djurišić, J. M. Elazar, and M. L. Majewski, Appl. Opt. **37**, 5271 (1998).
[22] J. M. McMahon, G. C. Schatz, and S. K. Gray, Phys. Chem. Chem. Phys. **15**, 5415 (2013).
[23] See http://rredc.nrel.gov/solar/spectra/am1.5/ASTMG173/ASTMG173.html for "Reference Solar Spectral Irradiance: ASTM G-173" (last accessed March 15, 2018).
[24] S. D. Lord, NASA Technical Memorandum 103957 (1992).
[25] See https://atran.sofia.usra.edu/cgi-bin/atran/atran.cgi for "Web-based input form for ATRAN" (last accessed March 15, 2018).
[26] T. Kasuya and R. Kawamura, Tenki **59**, 917 (2012) (in Japanese).